ARMY RESEARCH LABORATORY

Topology Optimization Based Lightweight Armor Development

by Dwight Hofstetter Jr., Rahul Gupta, and Robert Bitting

ARL-TR-5319 September 2010

Approved for public release; distribution is unlimited.

NOTICES

Disclaimers

The findings in this report are not to be construed as an official Department of the Army position unless so designated by other authorized documents.

Citation of manufacturer's or trade names does not constitute an official endorsement or approval of the use thereof.

Destroy this report when it is no longer needed. Do not return it to the originator.

Army Research Laboratory
Aberdeen Proving Ground, MD 21005-5066

ARL-TR-5319 **September 2010**

Topology Optimization Based Lightweight Armor Development

Dwight Hofstetter Jr.
Oak Ridge Institute for Science and Education (ORISE)

Rahul Gupta and Robert Bitting
Weapons and Materials Research Directorate, ARL

Approved for public release; distribution is unlimited.

REPORT DOCUMENTATION PAGE

Form Approved
OMB No. 0704-0188

Public reporting burden for this collection of information is estimated to average 1 hour per response, including the time for reviewing instructions, searching existing data sources, gathering and maintaining the data needed, and completing and reviewing the collection information. Send comments regarding this burden estimate or any other aspect of this collection of information, including suggestions for reducing the burden, to Department of Defense, Washington Headquarters Services, Directorate for Information Operations and Reports (0704-0188), 1215 Jefferson Davis Highway, Suite 1204, Arlington, VA 22202-4302. Respondents should be aware that notwithstanding any other provision of law, no person shall be subject to any penalty for failing to comply with a collection of information if it does not display a currently valid OMB control number.
PLEASE DO NOT RETURN YOUR FORM TO THE ABOVE ADDRESS.

1. REPORT DATE *(DD-MM-YYYY)*	2. REPORT TYPE	3. DATES COVERED (From - To)
September 2010	Final	June 2010–August 2010

4. TITLE AND SUBTITLE
Topology Optimization Based Lightweight Armor Development

5a. CONTRACT NUMBER

5b. GRANT NUMBER

5c. PROGRAM ELEMENT NUMBER

6. AUTHOR(S)
Dwight Hofstetter Jr.*, Rahul Gupta, and Robert Bitting

5d. PROJECT NUMBER

5e. TASK NUMBER

5f. WORK UNIT NUMBER

7. PERFORMING ORGANIZATION NAME(S) AND ADDRESS(ES)
Blast Protection Branch, Protection Division
U.S. Army Research Laboratory
ATTN: RDRL-WMP-F
Aberdeen Proving Ground, MD 21005-5066

8. PERFORMING ORGANIZATION REPORT NUMBER

9. SPONSORING/MONITORING AGENCY NAME(S) AND ADDRESS(ES)
U.S. Army Research Laboratory
ATTN: RDRL-WMP-F
Aberdeen Proving Ground, MD 21005-5066

10. SPONSOR/MONITOR'S ACRONYM(S)
ARL-TR-5319

11. SPONSOR/MONITOR'S REPORT NUMBER(S)

12. DISTRIBUTION/AVAILABILITY STATEMENT
Approved for public release; distribution is unlimited.

13. SUPPLEMENTARY NOTES
*Oak Ridge Institute for Science and Education (ORISE)

14. ABSTRACT
Improvised Explosive Devices (IEDs) present a constant and continually changing threat to the vehicles on the modern battlefield. Continual reengineering is needed to keep up with these threats and to safeguard the vehicles and the warfighters. To achieve this, protection kits need to be added to the vehicles. However, armor kits are a concession between maximum strength and minimum weight. Livermore Software Topology Optimization (LS-OPT)/Topology optimization software takes into account size, shape, and topology by designing for a uniform internal energy density in the structure while keeping the mass constrained. The user needs to develop a model matching the allowable limits of the desired part with a finite element analysis preprocessor. Then, the model is imported into LS-OPT/Topology and specific design limits are set. The program makes constant iterations until a tolerance with respect to the design limit (in this case mass fraction) is reached, or the amount of iterations have surpassed the set boundary. This paper explores the practical usage of LS-OPT/Topology that can be utilized by the engineers at U.S. Army Research Laboratory (ARL) to improve the modeling and simulation capabilities in the area of vehicle protection leading to Soldier survivability.

15. SUBJECT TERMS
summer student, topology, optimization, LS-OPT/topology, armor

16. SECURITY CLASSIFICATION OF:			17. LIMITATION OF ABSTRACT	18. NUMBER OF PAGES	19a. NAME OF RESPONSIBLE PERSON
a. REPORT	b. ABSTRACT	c. THIS PAGE			Rahul Gupta
Unclassified	Unclassified	Unclassified	UU	34	19b. TELEPHONE NUMBER (*Include area code*) 410-278-6035

Standard Form 298 (Rev. 8/98)
Prescribed by ANSI Std. Z39.18

Contents

List of Figures **v**

List of Tables **vi**

Acknowledgments **vii**

1. Introduction/Background **1**

2. Theory **1**

2.1 Topology 1

2.2 Hybrid Cellular Automata (HCA) 2

2.2.1 Internal Energy Density (*6*, *7*) 3

2.3 Criteria for Evaluating Elements 3

2.3.1 Strain Hardening Modulus (*6*, *7*) 5

3. Operation **5**

3.1 LS-Prepost 5

3.2 Opening/Information 5

3.3 Cases 5

3.4 Problem 6

3.5 Method 6

3.6 Solution 6

3.7 View 6

4. Experiment **7**

4.1 Observation 7

4.2 Hypothesis 7

4.3 Procedure 7

5. Results **8**

5.1 The 0.75 Mass Fraction (Coarse Mesh) 9

5.2 The 0.50 Mass Fraction (Coarse Mesh) 11

5.3 The 0.4 Mass Fraction (Coarse Mesh) 13
5.4 The 0.75 Mass Fraction (Fine Mesh) 15
5.5 The 0.50 Mass Fraction (Fine Mesh) 17

6. Summary and Conclusion **18**

7. References **19**

List of Symbols, Abbreviations, and Acronyms **20**

Distribution List **21**

List of Figures

Figure 1. Hybrid cellular automata based topology optimization method.....2
Figure 2. Hybrid cellular automata based topology optimization flowchart (*6, 7*).....3
Figure 3. Topology optimization method simulation model. 8
Figure 4. Coarse mesh 0.75 mass fraction density redistribution. 10
Figure 5. Coarse mesh 0.75 mass fraction total internal energy density. 10
Figure 6. Coarse mesh 0.75 mass fraction initial vs. optimized. 11
Figure 7. Coarse mesh 0.75 mass fraction density redistribution. 11
Figure 8. Coarse mesh 0.5 mass fraction density redistribution. 12
Figure 9. Coarse mesh 0.5 mass fraction total internal energy density. 12
Figure 10. Coarse mesh 0.5 mass fraction initial vs. optimized. 13
Figure 11. Coarse mesh 0.5 mass fraction density redistribution. 13
Figure 12. Coarse mesh 0.4 mass fraction density redistribution. 14
Figure 13. Coarse mesh 0.4 mass fraction total internal energy density. 14
Figure 14. Coarse mesh 0.4 mass fraction initial vs. optimized. 14
Figure 15. Coarse mesh 0.4 mass fraction density redistribution. 15
Figure 16. Fine mesh 0.75 mass fraction density redistribution. 15
Figure 17. Fine mesh 0.75 mass fraction total internal energy density. 16
Figure 18. Fine Mesh 0.75 mass fraction initial vs. optimized. 16
Figure 19. Fine mesh 0.75 mass fraction density redistribution. 16
Figure 20. Fine mesh 0.5 mass fraction initial vs. optimized 17
Figure 21. Fine mesh 0.5 mass fraction density redistribution. 17

List of Tables

Table 1. Coarse mesh (1 × 1 × 1 in, non-linear). 9
Table 2. Fine mesh (0.5 × 0.5 × 0.5 in, non-linear). 9

Acknowledgments

The author wishes to acknowledge the mentorship of Dr. Rahul Gupta, Blast Protection Branch, U.S. Army Research Laboratory (ARL).

INTENTIONALLY LEFT BLANK.

1. Introduction/Background

Today's enemy has been relying heavily on Improvised Explosive Devices (IEDs) to defeat vehicles used by the U.S. and its allies. Thus, there is a push to rush the immediate armoring of less protected vehicles. However, with added armor comes added weight, less maneuverability, and more frequent maintenance. It is the mission of U.S. Army Research Laboratory (ARL) to develop suitable designs that take into account the practicality of superior strength with the necessity of lighter weight. The problem that engineers face is determining how material can be removed without jeopardizing the integrity of the structure. Another aspect for the engineer to consider is that each physical test of a vehicle's resistance to blast loading typically destroys the armor and/or the vehicle, making repeated tests both expensive and time consuming (*1*). In an effort to address the compromise between strength and weight while minimizing research expense, Livermore Software Topology Optimization (LS-OPT)/Topology appears to be a valuable tool for the development of lightweight armor kits. It is one of the first to explore the field of non-linear problems with dynamic loading. Physical nonlinearities are abundant in the process of a blast event (*2*). The topology optimization in the context of impact analysis is a very complex problem due to non-linear interactions among material non-linearities, geometry, and the transient nature of the boundary conditions. Conventional methods are not practical for solving these non-linear topology optimization problems due to the high computational cost and the lack of sensitivity information (*3*).

2. Theory

2.1 Topology

LS-OPT/Topology is a novel optimization software that optimizes the size, shape, and topology of a model through reconstruction. Topology is an important factor in this process, because it deals with the material as well as the material properties. Figure 1 demonstrates an example of the topology optimization process. Topology is defined as a field in mathematics which focuses on an object's spatial properties as they are preserved during deformations such as bending or twisting but not to include tearing (*4*). The topology aspect of LS-OPT/Topology essentially takes a raw or developed lump of clay then reshapes it to optimize the piece's structural integrity while keeping it within its specific constraints. In the same manner, the program will also minimize the size and shape of the piece by removing cells from which it is made; yet the program will not cut the model into more than one piece. Design for structural topology optimization is a method of distributing material within a design domain of prescribed dimensions. This domain is discretized into a large number of elements in which the

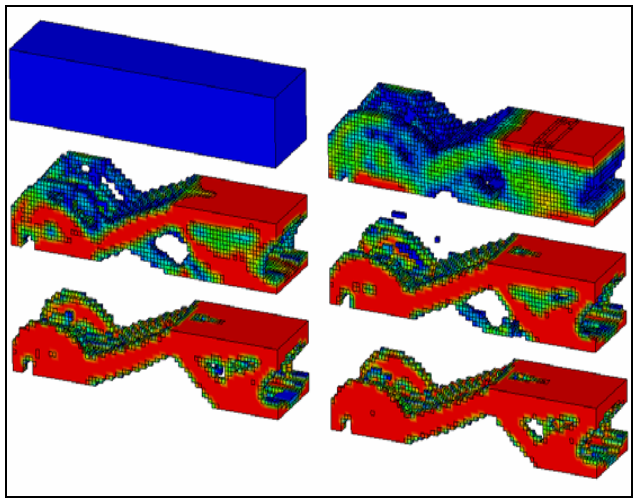

Figure 1. Hybrid cellular automata based topology optimization method.

optimization algorithm removes, adds, or maintains the amount of material. The resulting structure maximizes a prescribed mechanical performance while satisfying functional and geometric constraints (*2*).

2.2 Hybrid Cellular Automata (HCA)

Over the years, several methods have been developed to analyze the mathematical field of topology. The LS-OPT/Topology developers believe that the most successful method for analyzing dynamically loaded problems is HCA. A cellular automaton (CA) is a collection of "colored" cells on a grid of a specified shape that evolves through a number of discrete time steps according to a set of rules based on the states of neighboring cells (*5*). However, for the structural optimization problems, the state of a cellular automaton is defined by rules that combine the local neighborhood information with the field variables that are calculated globally (*6*, *7*), which makes the method a hybrid. The globally calculated field variables refer to those held within the entire model. Control rules drive a defined field variable to an optimum state or set point. The expression for the field variable and the value of the set point are derived from the optimality conditions of the structural design problem. Among different topology optimization algorithms, the hybrid cellular automaton HCA method has proven to be efficient and robust in problems involving large, plastic deformations (*2*). The idea of HCA can be seen in equation 1.

$$U_i = \sum_{j=1}^{n} U_j \Big/ \sum_{j=1}^{n} 1. \tag{1}$$

(U_i) = energy density of ith cellular automata lattice
n= amount of neighbors/adjacent cells
(The number one is in the denominator so the denominator sums to n.)

2.2.1 Internal Energy Density (*6*, *7*)

In the context of HCA, the field variables are subjected to the neighborhood update rule first and then the design variables are updated. This process is iterated until equilibrium is established among all state variables (*6*, *7*). HCA is a simple yet effective method for analyzing the topology of a model as can be seen in figure 2.

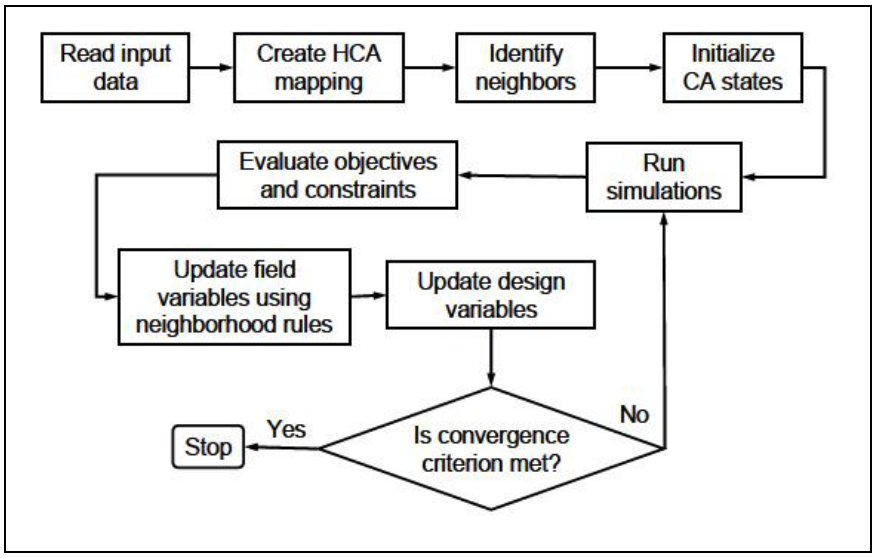

Figure 2. Hybrid cellular automata based topology optimization flowchart (*6*, *7*).

2.3 Criteria for Evaluating Elements

The basic principles behind how LS-OPT/Topology functions are easy to follow. The topology design problem is defined by the allowable geometric domain, how the part will be used, and properties of the part (*8*). These aspects are assigned in the initial LS-Prepost modeling. When the model is built within LS-Prepost, it is required that it be constructed using PIECEWISE_LINEAR_PLASTICITY using only eight-noded solid elements (*8*). A design variable is directly linked to each of these material elements such that each cell has its own material model (*8*). The objective for optimization is to obtain a maximum uniform internal energy density among all of these elements (*7*, *9*). The formulation of the optimization problem can be seen in equations 2 and 3.

$$\min_{x} \sum_{i=}^{N} \sum_{j=1}^{L} \left(w_j U_j(x_i) - U_j^* \right), \tag{2}$$

U = energy density of the ith element
w= weighted parameter
U*= internal energy set point

L= amount of load cases
x = relative density/design variable
Optimization problem (*6, 7*)

$$\begin{aligned} subject\ to: \sum_{i=1}^{N} \rho(x_i)V_i \le M^* \\ x_{\min} \le x_i \le 1.0. \end{aligned} \tag{3}$$

V_i = volume of the ith element
ρ = density of the material
M*= updated mass of the structure
x = relative density/design variable

Optimization Problem Constraints (*6, 7*)

The solid isentropic material with a penalization model is used to interpolate the material properties as can be seen in the equations 4, 5, and 6.

$$\rho(x) = x\rho_0 \tag{4}$$

ρ = density of the material
0 = refers to the base material properties
x = relative density/design variable

2.3.2 Density (*6, 7*)

$$E(x) = x^p E_0 \tag{5}$$

E = Young's modulus
0 = refers to the base material properties
x = relative density/design variable
p= material linearity exponent

Young's Modulus (*6, 7*)

$$\sigma(x) = x^q \sigma_0 \tag{6}$$

σ = yield stress
0 = refers to the base material properties
x = relative density/design variable
q= material non-linearity exponent

Yield Stress (*6, 7*)

$$E_h(x) = x^q E_{h0} \tag{7}$$

E_h = strain hardening modulus

0 = refers to the base material properties
x = relative density/design variable
q= material non-linearity exponent

2.3.1 Strain Hardening Modulus (*6, 7*)

Internal energy most often consists of elastic and plastic deformations. By decreasing the mass of the entire model, an increase in the total internal energy per total mass can be obtained (*8*). When the blast pressure wave hits the targeted structure, the fluids kinetic energy is transformed into strain energy (SE) inside the solid medium. Maximum attenuation is reached when SE is maximized. Along with an optimum use of material, this condition is satisfied when SE is uniformly distributed in the design domain (*2*). When setting LS-OPT/Topology, several constraints can be set such as the number of design iterations, the desired mass fraction, and minimum density fraction before deleting an element. However, such constraints as maximum displacement are not accounted for within the current version of the LS-OPT/Topology software.

3. Operation

3.1 LS-Prepost

Operating the LS-OPT/Topology software is quite simple once the user becomes familiar with the operational concepts. First, a user must create a model in LS-Prepost which will set the limit constraints for the final optimized model. The model must be created using the PEICEWISE_LINEAR_PLASTICITY material with eight-noded solid elements and it must also be defined using "*Part". A user can include holes in the piece and if extrusions in the final model are desired the user can specify them in LS-Prepost.

3.2 Opening/Information

As with other software, LS-OPT/Topology's graphical user interface (GUI) can be opened from the file pull down menu. When the GUI window appears, the first item the user sees is the "information tab" with license and working directory information as well as a place to insert a problem description. The problem description is used for reference so anything can be written.

3.3 Cases

The next tab titled "cases" is where all of the input file information will be inserted. First a user must select the "new" button at the bottom of the window. In the "edit cases" pop up window a "general" tab will be selected. The user must create a name for the case as well as specify the weight which is simply a scaling factor if multiple loads are used. One of two types of analysis need to be selected: linear or non-linear. At this point the model that was created in LS-PrePost

can be imported into the program by browsing the input file name. LS-OPT/Topology requires a Livermore Software Dynamic Analysis (LS-DYNA) executable to solve which can be specified by browsing the execution command. Advanced users typically modify the "scheduling" tab by choosing to limit the number of concurring jobs, choosing a Queue system, and setting an environmental variable. The default settings on these options are sufficient for this experiment. When done, the user can select the "ok" button to finish the selection.

3.4 Problem

After selecting the "problem" tab a design-part id needs to be specified. The design-part identification is a means of referring to the place where all elements in the design domain have been placed in the LS-DYNA input deck. This reference number can be found in the model's viewing window. If the LS-Prepost model has an extrusion specified, the extrusion set number can be inserted into the extrusion set box. On the bottom of the "problem" tab is a box labeled mass fraction. This refers to the amount of material that is desired to be eliminated where a value of 1 would conserve the original model and a value of 0 would remove the entire model.

3.5 Method

Under the method tab is the termination criteria. The most often used termination criteria is the number of design iterations. LS-OPT/Topology will terminate when this number of iterations is reached. The convergence tolerance terminates the program when the topology begins making few changes. This is controlled by the density redistribution history variable. The proximity tolerance is based on the uniformity of neighboring elements. Elements with a density less than the minimum density fraction specified in the minimum density fraction box will be deleted on a given iteration.

3.6 Solution

After selecting the "run" tab, the only visible button is "run". Upon clicking on this button, the user will be prompted to save the solution. A storage location and a name are given to the run, "ok" is selected, and the solution begins. Each iteration has a percent completion bar displayed at the top of the page and an engine output display is visible at the bottom. At any time the run can be stopped and deleted or stopped to be restarted later.

3.7 View

The "view" tab allows a user to see a graph of the density redistribution as well as a graph of the total internal energy density. As the number of iterations increases the graphs readjust to show the new data. From the "view" tab a user can also open LS-Prepost to post process the iterations displaying the changes that have been made to the model. The iterations can be viewed individually or simultaneously in a window with regards to density or internal energy density.

4. Experiment

4.1 Observation

After seeing LS-OPT/Topology presented, or solving example problems from the user's manual, it can be concluded that this technology could be used in the design and analysis of blast protection. The examples within the LS-OPT/Topology user's manual exhibited examples solved with beams but plates are also feasible models.

4.2 Hypothesis

It is hypothesized that in the utilization of LS-OPT/Topology for the designing and testing of armor plates, a model containing more initial elements will be developed into a more accurate optimized piece compared to a model containing fewer but larger initial elements. Since LS-OPT/Topology removes whole elements, removing several smaller elements would be more precise and thorough than removing larger elements.

4.3 Procedure

To test the hypothesis, it was decided that a plate under pressure loading would be tested. Figure 3 demonstrates the model with dimension, loading, boundary conditions and material properties. The plate was 48 × 48 × 6 in with boundaries set along opposite edges with a bottom pressure loading in order to imitate a blast load from an underbody IED. The plate was assigned a mass density of 7850 kg/m^3, a Young's modulus of 2.068 ×10^{11} Pa and a yield stress of 0.27 MPa. The first, second, third, and fourth effective strain values were 0.0, 0.0055, 0.0152, and 0.0248 respectively. The fifth, sixth, seventh, and eighth effective strain values were 0.0627, 0.16, 0.28, and 0.42, respectively. The first, second, third, and fourth corresponding yield stress value to effective strain values were 7.922 × 10^8 Pa, 9.23 × 10^8 Pa, 9.610 × 10^8 Pa, and 9.830 × 10^8 Pa, respectively. The fifth, sixth, seventh, and eighth corresponding yield stress value to effective strain values were 1.029 × 10^8 Pa, 1.077 × 10^9 Pa, 1.098 × 10^9 Pa, and 1.104 × 10^9 Pa, respectively.

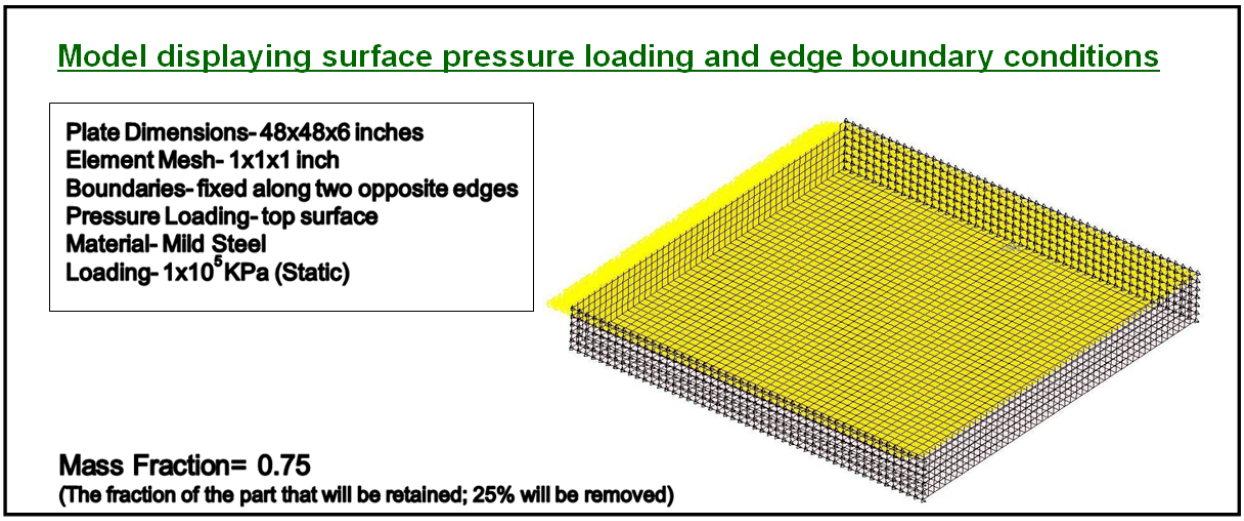

Figure 3. Topology optimization method simulation model.

The only difference between the two plates was that the course mesh plate was created with 1 × 1 × 1 in elements where the fine mesh plate was created with 0.5 × 0.5 × 0.5 in elements (finer mesh). In the experiment, the only variable that was changed was the mass fraction. Each plate would be optimized for: (1) 0.75 mass fraction, (2) 0.5 mass fraction, and (3) 0.25 mass fraction. However, the solutions ended up including 0.4 mass fraction, 0.5 mass fraction, and 0.75 mass fraction. Preliminary solutions showed that under the operating system used, an initial iteration could not be completed for a 0.25, 0.3, or a 0.35 mass fraction on the coarse mesh plate; therefore, a 0.4 mass fraction was used. Each solution consisted of a non-linear analysis with the number of iterations set to 100. Other values were left as defaults. Most solutions were made overnight due to the length of time required to make all of the iterations.

5. Results

Each solution ended with a different number of iterations and all ended with error terminations due to negative volume. Negative volume is often the result of deforming an element so extensively that it is inverted inside out. Tables 1 and 2 summarize the iteration results.

Table 1. Coarse mesh (1 × 1 × 1 in, non-linear).

Mass Fraction	Vertical Deformation (in)	Initial Mass (kg)	Final Mass (kg)	No. of Iterations		Density Redistribution	Internal Energy Density (KN/m^2)
0.75	0.35	1778.42	1333.84	11	Initial	0.072	4.6E+011
					Final	0.015	3.1E+011
0.5	0.63	1778.42	889.149	7	Initial	0.062	9E+011
					Final	0.055	5.5 E+011
0.4	0.87	1778.42	711.319	5	Initial	0.06	3.5E+012
					Final	0.055	0.75E+012

Table 2. Fine mesh (0.5 × 0.5 × 0.5 in, non-linear).

Mass Fraction	Vertical Deformation (in)	Initial Mass (kg)	Final Mass (kg)	No. of Iterations		Density Redistribution	Internal Energy Density (KN/m^2)
0.75	0.5118	1778.42	1333.84	4	Initial	0.072	4.52E+012
					Final	0.072	3.69E+012
0.5	1.142	1778.42	889.149	2	Initial	N/A	N/A
					Final	N/A	N/A
0.4	N/A	1778.42	N/A	0	Initial	N/A	N/A
					Final	N/A	N/A

Note: N/A = not applicable.

5.1 The 0.75 Mass Fraction (Coarse Mesh)

The 0.75 mass fraction solution of the coarse mesh plate ended in an error termination due to a negative volume on its eleventh iteration. The density distribution increased to 0.072 then leveled off to around 0.015 (figure 4). The total internal energy density dropped from 4.6×10^{11} KN/m^2 and leveled off at 3.1×10^{11} KN/m^2 (figure 5). Figure 6 shows that the final iteration (right) had symmetrical crescent shapes removed from the blue surface of the plate. Figure 7 demonstrates the mass fraction density redistribution.

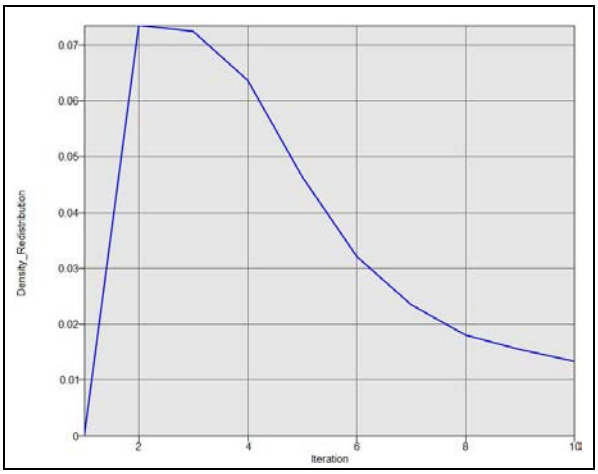

Figure 4. Coarse mesh 0.75 mass fraction density redistribution.

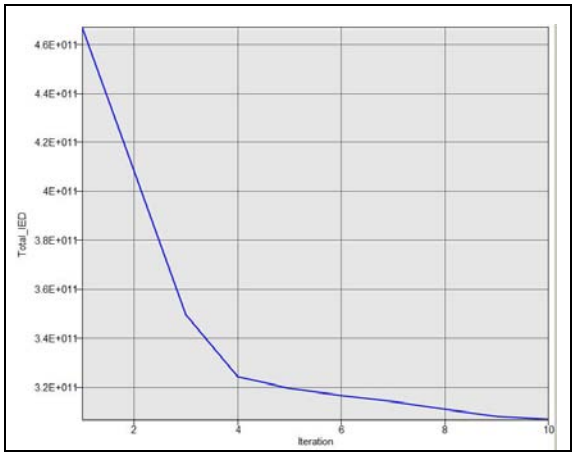

Figure 5. Coarse mesh 0.75 mass fraction total internal energy density.

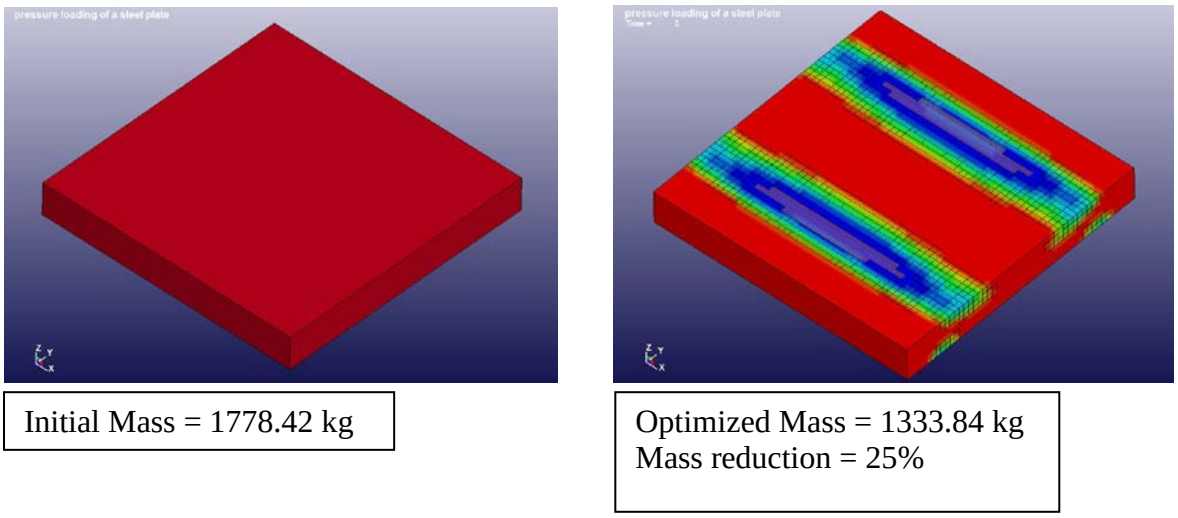

Figure 6. Coarse mesh 0.75 mass fraction initial vs. optimized.

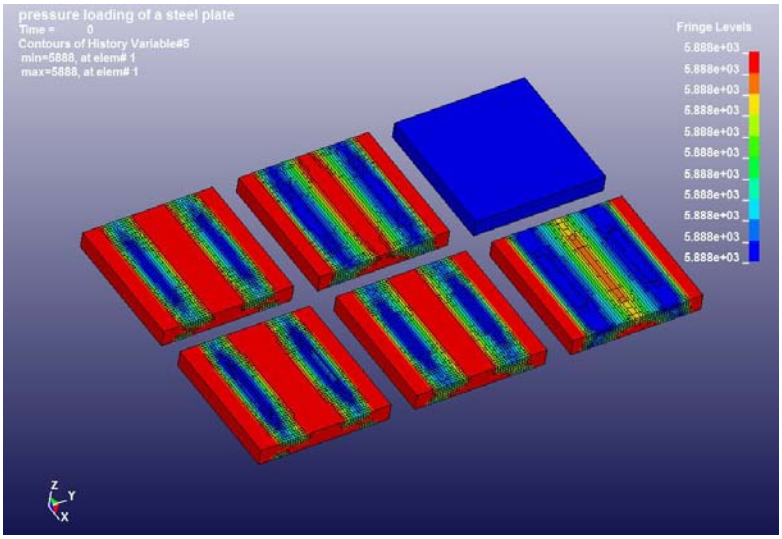

Figure 7. Coarse mesh 0.75 mass fraction density redistribution.

5.2 The 0.50 Mass Fraction (Coarse Mesh)

The 0.5 mass fraction solution of the coarse mesh plate ended in an error termination due to a negative volume on its seventh iteration. The density distribution increased to 0.062 then leveled off to around 0.055 (figure 8). The total internal energy density dropped from 9×10^{11} KN/m^2 and leveled off at 5.5×10^{11} KN/m^2 (figure 9). Figure 10 demonstrates the final iteration (right) had symmetrical crescent shapes removed from the blue surface of the plate. Figure 11 demonstrates the mass fraction density redistribution.

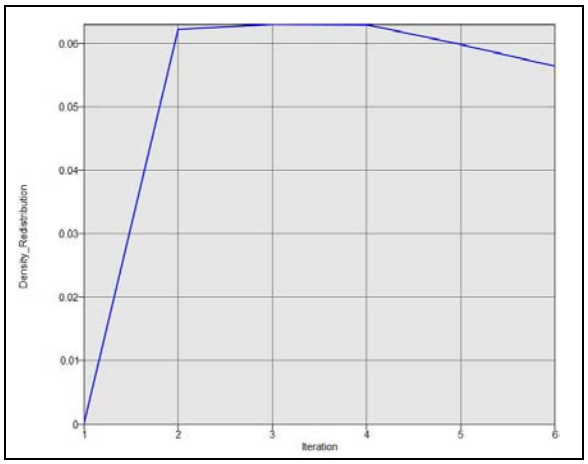

Figure 8. Coarse mesh 0.5 mass fraction density redistribution.

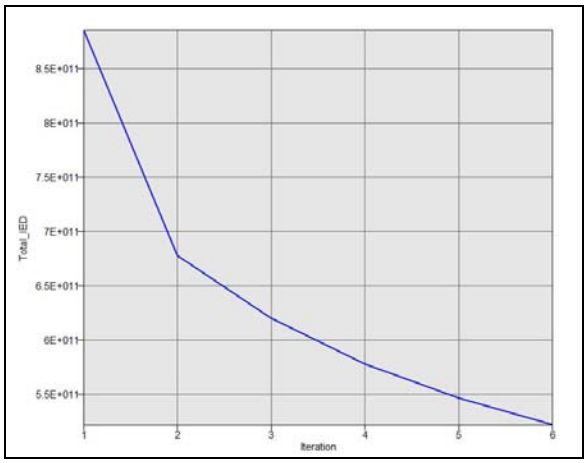

Figure 9. Coarse mesh 0.5 mass fraction total internal energy density.

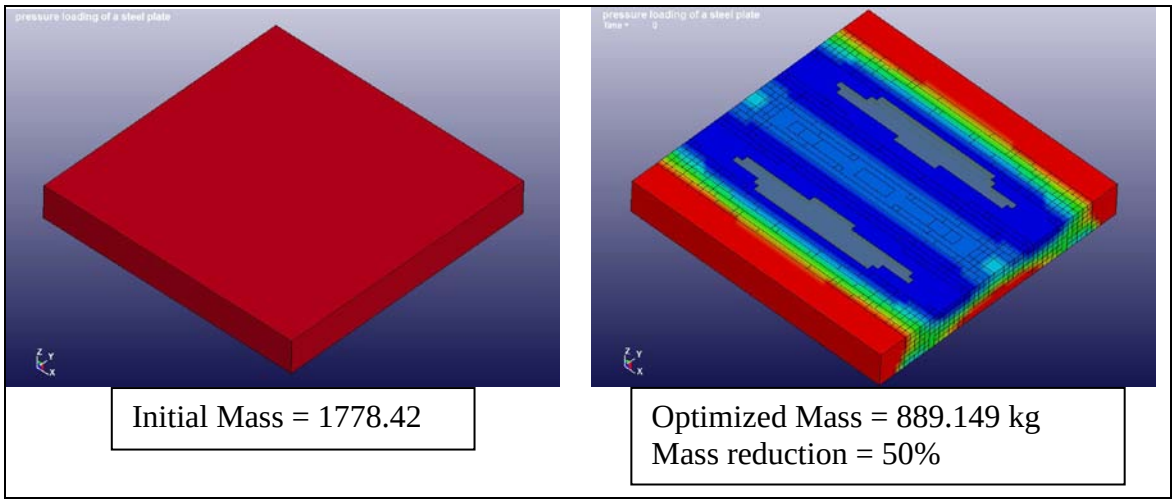

Figure 10. Coarse mesh 0.5 mass fraction initial vs. optimized.

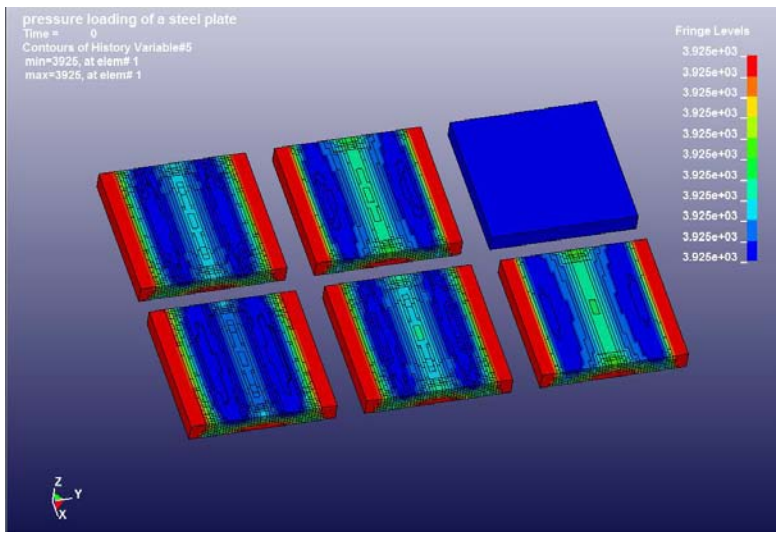

Figure 11. Coarse mesh 0.5 mass fraction density redistribution.

5.3 The 0.4 Mass Fraction (Coarse Mesh)

The 0.4 mass fraction solution for the coarse mesh plate ended in an error termination due to a negative volume on its fifth iteration. The density distribution increased to 0.06 then leveled off to around 0.055 (figure 12). The total internal energy density dropped from 3.5×10^{12} KN/m^2 and leveled off at 0.75×10^{12} KN/m^2 (figure 13). Figure 14 demonstrates that the final iteration (right) had symmetrical crescent shapes removed from the blue surface of the plate. Figure 15 demonstrates the mass fraction density redistribution.

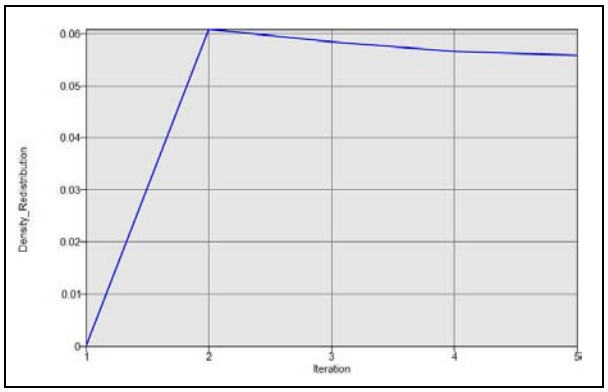

Figure 12. Coarse mesh 0.4 mass fraction density redistribution.

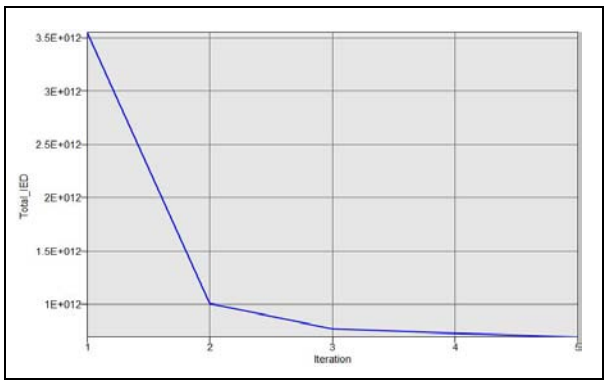

Figure 13. Coarse mesh 0.4 mass fraction total internal energy density.

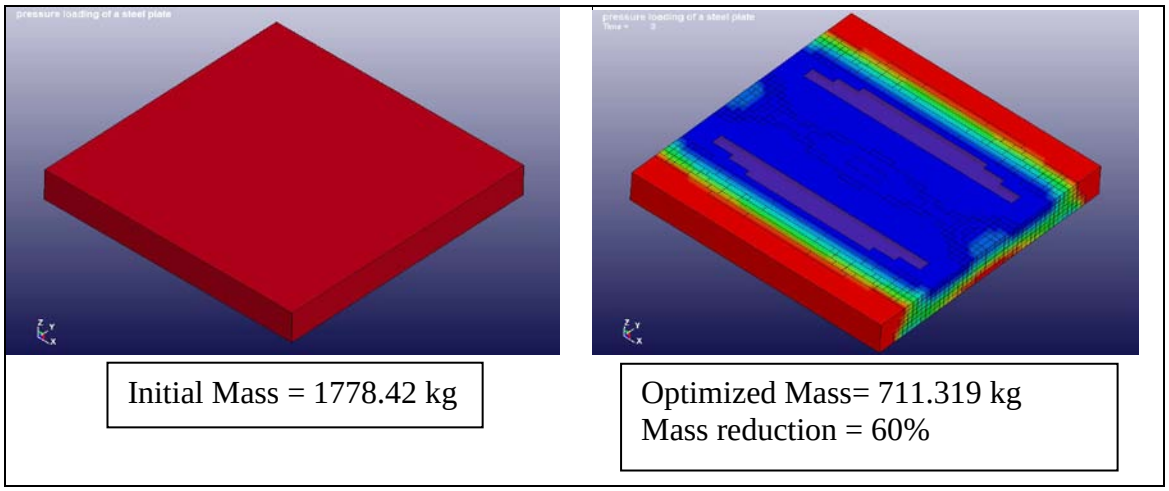

Figure 14. Coarse mesh 0.4 mass fraction initial vs. optimized.

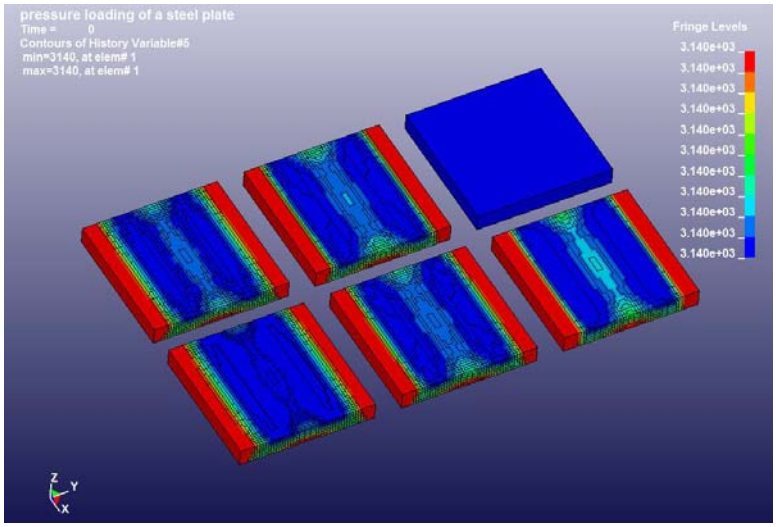

Figure 15. Coarse mesh 0.4 mass fraction density redistribution.

5.4 The 0.75 Mass Fraction (Fine Mesh)

The 0.75 mass fraction solution of the fine mesh plate ended in an error termination due to a negative volume on its fourth iteration. The density distribution increased to 0.072 then leveled off as shown in figure 16. The total internal energy density dropped from 4.52×10^{12} KN/m^2 and steadily declined as shown in figure 17. Figure 18 demonstrates that the final iteration (right) did not have any material removed at the time of testing. Figure 19 demonstrates the mass fraction density redistribution. Solving the 0.75 mass fraction with the fine mesh took roughly 2 days (46 h) to complete.

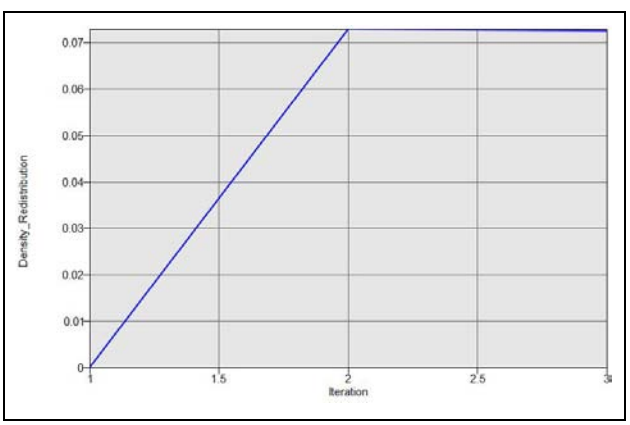

Figure 16. Fine mesh 0.75 mass fraction density redistribution.

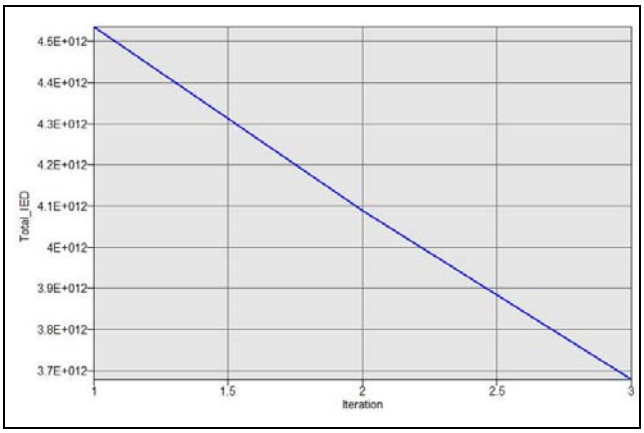

Figure 17. Fine mesh 0.75 mass fraction total internal energy density.

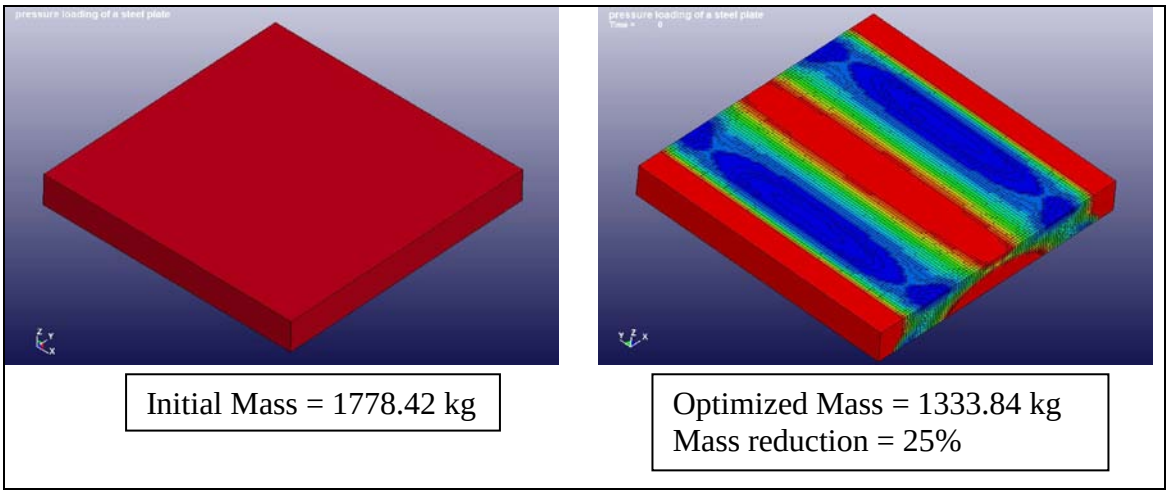

Figure 18. Fine Mesh 0.75 mass fraction initial vs. optimized.

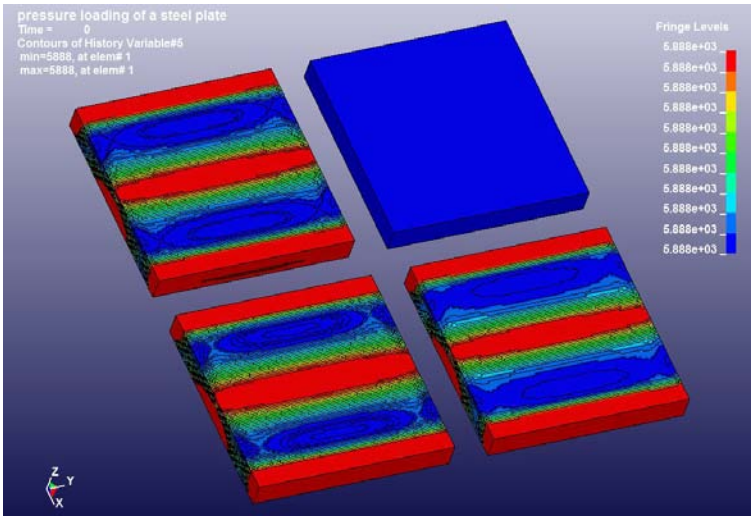

Figure 19. Fine mesh 0.75 mass fraction density redistribution.

5.5 The 0.50 Mass Fraction (Fine Mesh)

The 0.5 mass fraction solution of the fine mesh plate ended in an error termination due to a negative volume on its second iteration. Since the program was unable to begin to remove material as of the second iteration, neither the density redistribution nor the total internal energy density graphs could be drawn. However, the initial iteration was able to produce an analyzed plate as shown in figure 20. Figure 21 demonstrates the mass fraction density redistribution.

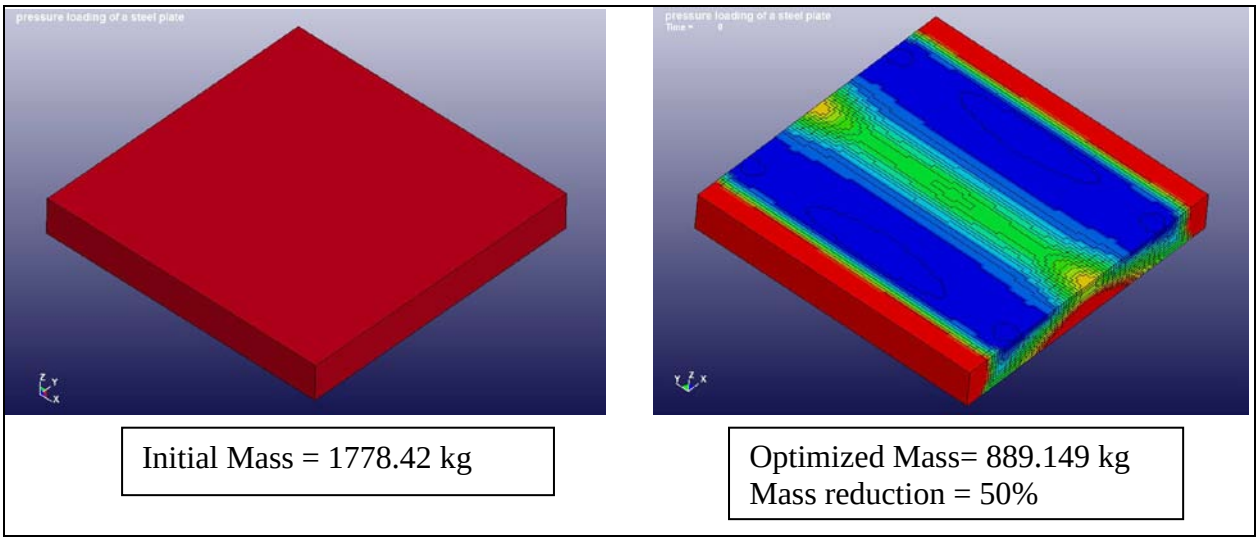

Figure 20. Fine mesh 0.5 mass fraction initial vs. optimized

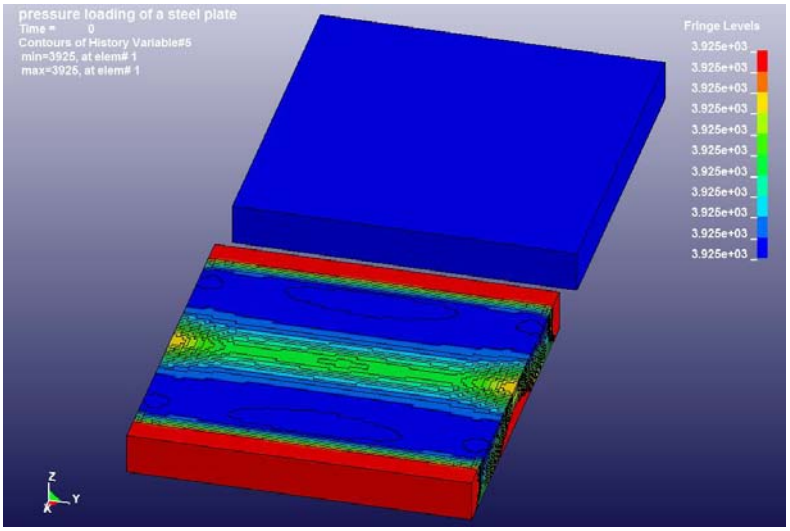

Figure 21. Fine mesh 0.5 mass fraction density redistribution.

The 0.4 mass fraction solution of the fine mesh plate ended in an error termination due to a negative volume on its first iteration. Since the first iteration was not completed, no data can be viewed concerning its potential form.

6. Summary and Conclusion

Initially, it was believed that an error termination was acceptable since most solutions displayed an optimized model before they were terminated. However, it was discovered subsequently that the coarse mesh plate used for this experiment can be solved to completion using a mass fraction of 0.25 since LSTC was using massively parallel processing (MPP) on a Linux operating system while the ARL simulation experiment was conducted using symmetric multiprocessing (SMP) on a Windows operating system. If the experiment had been successful and every case solved through completion, each resulting model would show a plate that would progressively reduce mass in order to reflect the required mass fraction. A model with a finer mesh should portray a more accurate depiction of the optimized form. In the experiment, the solutions with lower mass fractions ended with less number of iterations, most likely because the program had more mass that was required to be removed so that the initial removal could be substantial. The solutions of the model containing the finer mesh also ended with a less number of iterations. However, the iterations themselves took much longer to complete than those of the coarser mesh. This is possibly due to the fact that more elements had to be removed to equal the amount of larger elements removed from the coarser meshed model. Upon completion of the experimental study, further analysis will be presented in future publications.

7. References

1. Optimization of an Armored Plate for Light Armored Vehicles Subjected to Blast Loading. Red Ceder Technologies, Inc. East Lansing, Michigan, 2009.

2. Goetz, J. C.; Tan, H.; Renaud, J. E.; Tovar, A. Structural Topology Optimization for Blast Mitigation Using Hybrid Cellular Automata. *2009 Ground Vehicle Systems Engineering and Technology Symposium (GVSETS)*. 2009.

3. LSTC, Goel, T. Topology Optimization using LS-OPT/Topology. http://www.lsoptsupport.com/news/topology-optimization-using-ls-optae-topology (accessed 2010).

4. Wikipedia, Topology, http://en.wikipedia.org/wiki/Topology (accessed 2010).

5. Weisstein, E. W. Mathworld, Cellular Automaton. http://mathworld.wolfram.com/CellularAutomaton.html (accessed 2010).

6. Goel, T.; Roux, W. *LS-OPT/Topology A Topology Optimization Tool for LS-DYNA: User's Manual:* Livermore Software Technology Corporation, Livermore, CA, 2009.

7. Goel, T.; Roux, W.; Stander, N. A Topology Optimization Tool for LS-DYNA Users: LS-OPT/Topology. *7th European LS-DYNA Conference*. 2009.

8. Roux, W.; Goel, T.; Björkevik, D. LS-OPT/Topology Version 1. *11th International LS-DYNA Users Conference*. 2010.

9. Mayer, R. R.; Kikuchi, N.; Scott, R. A. Application of Topological Optimization Techniques to Structural Crashworthiness. *International Journal for Numerical Methods in Engineering* **1996**, *39*, 1383–1403.

10. *LS-DYNA Keyword User's Manual: Volume 1*: Livermore Software Technology Corporation, Livermore, CA, 2007.

List of Symbols, Abbreviations, and Acronyms

ARL	U.S. Army Research Laboratory
CA	cellular automaton
GUI	graphical user interface
HCA	Hybrid Cellular Automata
IEDs	Improvised Explosive Devices
LS-DYNA	Livermore Software Dynamic Analysis
LS-OPT	Livermore Software Topology Optimization
MPP	massively parallel processing
N/A	not applicable
SE	strain energy
SMP	symmetric multiprocessing

NO. OF COPIES	ORGANIZATION
1 (PDF only)	DEFENSE TECHNICAL INFORMATION CTR DTIC OCA 8725 JOHN J KINGMAN RD STE 0944 FORT BELVOIR VA 22060-6218
1	DIRECTOR US ARMY RESEARCH LAB IMNE ALC IMS 2800 POWDER MILL RD ADELPHI MD 20783-1197
1	DIRECTOR US ARMY RESEARCH LAB RDRL CIM L 2800 POWDER MILL RD ADELPHI MD 20783-1197
1	DIRECTOR US ARMY RESEARCH LAB RDRL CIM P 2800 POWDER MILL RD ADELPHI MD 20783-1197
	ABERDEEN PROVING GROUND
2	DIR USARL RDRL CIM P (BLDG 305)

NO. OF COPIES	ORGANIZATION
1	DIR US ARMY RESEARCH LAB RDRL D R SKAGGS 2800 POWDER MILL RD ADELPHI MD 20783-1197
2	US ARMY RESEARCH OFC D STEPP B LAMATTINA PO BOX 12211 RESEARCH TRIANGLE PARK NC 27709-2211
3	DARPA SPECIAL PROJECTS OFC TACTICAL TECHNOLOGY OFC W JOHNSON DEFENSE SCIENCE OFC S WAX ADVANCED TECHNOLOGY OFC D HONEY 3701 N FAIRFAX DR ARLINGTON VA 22203-1714
1	DIR DTRA MSC 6201 8725 JOHN J KINGMAN RD FORT BELVOIR VA 22060-6201
1	DIR DEFENSE INTELLIGENCE AGENCY TA 5 K CRELLING WASHINGTON DC 20310
1	COMMANDER US ARMY MATERIEL CMD AMSMI INT 5001 EISENHOWER AVE ALEXANDRIA VA 22333-0001
1	COMMANDER US ARMY TACOM PM COMBAT SYSTEMS SFAE GCS CS 6501 ELEVEN MILE RD WARREN MI 48397-5000

NO. OF COPIES	ORGANIZATION
3	PM FCS BCT MSI SFAE GCS UA P CAG S GRIEG T MCKHEEN 6501 ELEVEN MILE RD WARREN MI 48397-5000
1	COMMANDER US ARMY TACOM PEO CS & CSS PM LIGHT TACTICAL VHCLS SFAE CSS LT M1114 MGR 6501 ELEVEN MILE RD WARREN MI 48397-5000
1	COMMANDER US ARMY AMCOM AVIATION APPLIED TECH DIR J SCHUCK FT EUSTIS VA 23604-5577
4	COMMANDER NAVAL SURFACE WARFARE CTR CARDEROCK DIVISION R PETERSON CODE 2120 R CRANE CODE 6553 T BURTON CODE 667 U SORATHIA C WILLIAMS CODE 6551 WEST BETHESDA MD 20817-5700
13	COMMANDER US ARMY TACOM AMSTA TR R S KNOTT D DICEASURE J BENNETT D HANSEN AMSTA JSK E BARSHAW M CHAIT D TEMPLETON L PROKURAT-FRANKS AMSTA TR D D OSTBERG L HINOJOSA S HODGES C FILAR AMSTA CS SF F SCHWARZ WARREN MI 48397-5000

NO. OF COPIES	ORGANIZATION
1	OFC OF NAVAL RESEARCH J KELLY 3701 N FAIRFAX DR ARLINGTON VA 22203-1714
1	MARINE CORPS SYSTEM CMD J BURNS 2200 LESTER ST. QUANTICO VA 22134
1	CENTRAL INTELLIGENCE AGENCY WINPAC/CWTG/GWET M DAN RM 4P07 NHB WASHINGTON DC 20505
1	DIR LANL F ADDESSIO MS B216 PO BOX 1633 LOS ALAMOS NM 87545
2	THE BOEING CO J CHILDRESS N GERKEN MS 84-69 PO BOX 3707 SEATTLE WA 98124 CAGE CODE 81205
6	BAE SYSTEMS M MIDDIONE G THOMAS D SCHADE R MUSANTE T PIKE M IWEN PO BOX 359 SANTA CLARA CA 95050 CAGE CODE 80212
3	BAE SYSTEMS R BRYNSVOLD W BALLATA J BRODY PO BOX 21099 MINNEAPOLIS MN 55421
2	BAE SYSTEMS T STEELE R SCIORTINO PO BOX 15512 YORK PA 17405-1512 CAGE CODE 06085

NO. OF COPIES	ORGANIZATION
6	GENERAL DYNAMICS LAND SYSTEMS G TEAL B CALDWELL PO BOX 1800 WARREN MI 48090-1800
1	U.S ARMY TANK-AUTOMOTIVE RESEARCH DEVELOPMENT AND ENGINEERING CENTER EMERGING TECHNOLOGIES AMSRD TAR R MS 263 RICHARD GOETZ WARREN MI 48397-5000
2	GENERAL DYNAMICS LAND SYSTEMS STERLING HEIGHTS COMPLEX JIM ERIDON TOM ZELEZNIK 38500 MOUND ROAD STERLING HEIGHTS MI 48310-3200
2	MARINE CORPS SCIENCE AND TECHNOLOGY OFFICE OF NAVAL RESEARCH LEE MASTROIANNI JEFF BRADEL ONE LIBERTY CENTER 875 NORTH RANDOLPH STREET, SUITE 1156B CODE 30 ARLINGTON VA 22203-1995
1	SHIP HULL, MECHANICAL & ELECTRICAL S&T DIV OFFICE OF NAVAL RESEARCH ONR334 ROSHDY GEORGE S. BARSOUM PHD PE 800 N QUINCY ST ARLINGTON VA 22217-5660

NO. OF COPIES	ORGANIZATION
	ABERDEEN PROVING GROUND
69	DIR US ARMY RESEARCH LAB RDRL CI RDRL LOA F M ADAMSON RDRL SL R COATES RDRL SLA B P KUSS J PLOSKONKA E HUNT B WARD RDRL SLB D R GROTE J POLESNE RDRL SLB E D LYNCH RDRL VTA J BORNSTEIN RDRL WM J SMITH L BURTON RDRL WML M ZOLTOSKI J NEWILL RDRL WML G W DRYSDALE S KUKUCK RDRL WML H B SORENSEN T FARRAND E KENNEDY L MAGNESS RDRL WMM A J WOLBERT M VANLANDINGHAM T BOGETTI B CHEESEMAN S GHIORSE C YEN R DOOLEY C FOUNTZOULAS RDRL WMM C R JENSEN M MAHER T JESSEN RDRL WMM D E CHIN B SCOTT S WALSH RDRL WMM E G GILDE P PATEL

NO. OF COPIES	ORGANIZATION
	RDRL WMM E J LASALVIA J SANDS RDRL WMM E P DEHMER RDRL WMM E J CAMPBELL RDRL WMM F K DOHERTY J MONTGOMERY RDRL WMP P BAKER RDRL WMP S SCHOENFELD M BURKINS RDRL WMP A B RINGERS RDRL WMP C T BJERKE RDRL WMP D T HAVEL V HERNANDEZ S HUG M KEELE D KLEPONIS J RUNYEON RDRDL WMP E M KLUSEWITZ W GOOCH D HACKBARTH E HORWATH C KRAUTHAUSER M LOVE RDRL WMP F N GNIAZDOWSKI E FIORAVANTE A FRYDMAN R GUPTA X HUANG D FOX R BITTING RDRL WMP G N ELDREDGE